

Contents lists available at ScienceDirect

# Journal of Constructional Steel Research

journal homepage: www.elsevier.com/locate/jcsr



# Check for updates

# Generalized spring model for steel bolts in tension considering uncertainty and loading speed

Zizhou Ding<sup>1</sup>, Ahmed Elkady \*,1

Department of Civil, Maritime and Environmental Engineering, University of Southampton, United Kingdom

#### ARTICLE INFO

# Keywords: Bolt fracture Bolt stiffness Bolted connections Ductility Numerical modeling Fracture uncertainty

#### ABSTRACT

Quantifying the rotational ductility of connections is key to studying the robustness of steel structures under extreme hazards and loading scenarios. In partial-strength bolted steel connections, the ultimate failure state is typically governed by bolt rupture. Simulating bolts using solid finite element models can be inconvenient for practical applications due to high computational demands and lengthy calibration procedures of the material damage parameters. Additionally, current bolt models do not capture the uncertainty associated with the bolt's elongation capacity. To address these challenges, a trilinear empirical spring model is proposed to accurately capture the bolt response up to failure while incorporating uncertainty; thereby supporting studies related to reliability and performance-based engineering. Two multi-variate empirical expressions are developed to predict the bolt's elastic stiffness and plastic elongation, as a function of its size, grade, grip, and thread lengths, providing improved accuracy across a wide range of bolt geometries. These expressions are derived from an extensive dataset of bolt assemblies under uniaxial tension, compiled from literature and supplemented by 200 newly tested specimens. The proposed model is applicable in finite element simulations employing axial connectors, numerical mechanics-based analyses, or design applications. The model is validated against experimental data at both the component and joint scales for various bolt grades and connection topologies, highlighting the impact of the bolt's response uncertainty on the joint-level ductility. The implications of high loading speed, representative of real dynamic hazard, on the bolt's response parameters are also quantified.

#### 1. Introduction

The rotational ductility of bolted steel connections is a key response characteristic that controls the design and the assessment of structural robustness under extreme loading scenarios arising from natural and man-made hazards such as collapse-level earthquakes, explosions, impacts, and progressive collapse following column loss. Design codes [3,10] provide explicit design provisions for the strength and stiffness of connections. On the other hand, there are no quantitative guidelines for the rotational ductility. Instead, rotational ductility is assumed to be adequate if material properties, geometric detailing, and fabrication guidelines are satisfied. In partial-strength bolted connections, bolt rupture is generally the controling failure mode. Empirical models that quantify the rotational ductility for partial-strength bolted connections are scarce [14,18]. This is attributed to the relatively limited experimental data for connections tested up to bolt failure, the complexity associated with the numerical simulation of bolt fracture, and the low

confidence in such simulations considering the intrinsic uncertainty associated with bolt failure due to geometrical and material variations.

The ductile behavior of partial-strength bolted steel connections, which are widely used in the steel construction practice, is mainly controlled by the plastic deformation of one or more of the connection's components (e.g., endplate bending, angle bending, column flange bending, beam local buckling, and column web panel zone shear distortion) as illustrated in Fig. 1. In such connections, the limit state representing complete loss of strength (i.e., failure) is mainly controlled by either bolt rupture, bolt stripping, bolt pull-through, weld failure, or plate tearing near heat affected zones. Weld failure may occur due to under-sized fillet welds, poor welding quality, strain concentration, or residual stresses [4,6]. Bolt stripping may occur under tension due to sub-grade materials, incompatible nut/bolt thread, and/or overtightening [9,13]. Pull-through failure can occur in very thin plates with oversized bolts. Plate tearing can take place near the heat-affected zone, particularly in thin plates, or plasticized regions under large

E-mail addresses: zd3e20@soton.ac.uk (Z. Ding), a.elkady@soton.ac.uk (A. Elkady).

 $<sup>^{\</sup>star}$  Corresponding author.

<sup>&</sup>lt;sup>1</sup> Address: Burgess Road, Boldrewood campus, Southampton SO17 7QF, UK.

strains or cyclic fatigue. These failure modes can be avoided through proper design, detailing, and fabrication. This leaves bolt rupture under tension or tension/shear as the primary failure mode, after sustaining excessive plastic deformation in the rest of the connection components. This damage hierarchy, consistent with Mode 2 and 3 yield mechanisms as per Eurocode 3 [10], is sought in design to ensure sufficient rotational ductility. Bolt elongation followed by bolt tensile rupture is the most common failure mode observed in endplate connections [14,16,30]. Contrary to bolt stripping, weld failure, and plate tearing, bolt rupture failure is predictable in theory, as it is based on connection mechanics, bolt geometry, and basic material properties. Accordingly, it is relatively simpler to simulate as part of computational simulations.

Bolt rupture develops as the bolt undergoes excessive plastic deformation and strain localization (necking) caused by void nucleation, growth, coalescence, and fracture formation. The fracture process depends on several factors such as the material type and loading conditions (i.e., stress state). Several continuum finite element (CFE) models were, and continue to be, proposed in the literature to simulate bolt behavior up to failure. In these models, various techniques are used to model the bolt geometry. On the extreme end, there is the highly detailed representation of the bolt assembly through the explicit modeling of the bolt head, thread, and nut geometry and corresponding variations in materials properties [21,24,39,46], as shown in Fig. 2(a). These types of models are generally used in studies concerned with studying thread clearance effects, simulating bolt thread stripping, or bolt preload through nut tightening. When it comes to predicting the bolt's forcedeformation or the joint's moment-rotation responses, the high computational cost of such sophisticated models is not justified and would not yield a noticeable difference compared to simpler models [24,39]. A simpler approach, and the most common, is to model the bolt as a single solid part with a simplified round head/nut and a smooth shank whose diameter varies equivalent to both the nominal and threaded portions, as demonstrated in Fig. 2(b). Finally, the simplest method is to represent the bolt using a wire -axial- connector element, as shown in Fig. 2(c). This method has a few limitations such as dominant shear loading scenarios, but it is computationally efficient, particularly when dealing with parametric or large-scale simulations.

For the solid models, the parameters of available phenomenological state-based damage models (the material's ductile fracture properties) are calibrated against tension/shear tests on bolt assemblies of a particular grade. This involves calibrating the parameters (primarily, critical plastic strains) defining damage initiation and evolution. Those are dependent on the material, the geometry, the stress state, and the loading rate. This calibration mainly involves trial and error iterations until the simulation results match that of the experiment. In these studies, fine mesh size is regularly employed and proposed; around 0.2-1.0 mm solid brick mesh elements. This, in addition to the fracture material model calibration procedure, leads to high computational cost. This is particularly critical in large studies involving system-level or parametric joint-level CFE simulations. Past studies also tend to develop models that are over-fitted to a case-specific test specimen/study. This over-fitting through trial-and-error procedures and model parameter tuning can introduce bias; consequently, the model accuracy, when extrapolated to other cases, becomes questionable. Notwithstanding these issues, when these calibrated bolt models are incorporated in connection-level simulations, the error in predicting the failure rotation ranges from 15 % to 40 % [36,40,48]. This is triggered by the unavoidable uncertainty associated with the variability of material properties and the fracture phenomenon. In reality, even for bolts from the same batch with exact class and specifications, the fracture point (elongation) can vary by up to 40 % [12,24,31]. Quantifying this uncertainty is key to developing design guidelines, numerical models, fragility function, and quantifying the reliability of structural systems at extreme limit states. To the best of the authors' knowledge, the uncertainty associated with bolt fracture has not been quantified in these past studies.

Within this context and considering the limitations of past studies, an empirical bolt model is proposed in this paper to simulate bolt rupture as part of CFE or component-based models, using the axial connector approach. This approach is meant to be practical by being 1) computationally efficient (does not need prior calibration, biased model tuning, sophisticated modeling, or significant simulation time), 2) simple to apply for a wide range of bolt geometries and grades, and 3) able to provide consistently accurate results across scales with quantifiable prediction intervals.

The paper is organized as follows: first, 200 high-strength bolts of different grades and geometric parameters were tested up to failure under varying loading speeds, up to 80mm/sec. Next, the experimental data is combined with those collected from the literature to create a multi-attribute dataset. Empirical expressions are developed using the compiled dataset to define the bolt's full-scale trilinear response including the uncertainty boundaries. These expressions address the limitations of current research with respect to generalization and accuracy. Thorough validations are presented with respect to individual bolt assemblies and full-scale joint tests, highlighting the model's accuracy and the potential implications of bolt response uncertainty. Finally, the effect of the loading speed (i.e., strain rate) on the bolt response parameters is quantified.

# 2. Characteristics of bolt geometry and F- $\Delta$ response

A bolt assembly consists of a head, nut, washers, threaded portion, and shank portion. Fig. 3(a) illustrates the parameters defining the bolt geometry which include the bolt's length  $(L_b)$ , nominal diameter  $(d_b)$ , grip length  $(L_g)$ , shank length  $(L_s)$ , and thread length  $(L_t)$ . Fig. 3(b) illustrates the typical force-elongation (F- $\Delta$ ) response fitted by a trilinear model. When a bolt assembly is under tension loading, it will initially undergo small movement until the threads are engaged (region noted as "s"). It will then develop uniform elastic deformation along the whole cross-section until reaching the yield force  $(F_v)$ . Plastic deformations are then concentrated within the threaded portion where plastic elongation continues to develop until reaching the ultimate force (Fu). Subsequently, the threaded portion will experience necking and strength degradation until the failure force ( $F_f$ ). The bolt's response is controlled by the yield, ultimate, and failure points. Therefore, a trilinear model is introduced to capture the main characteristics of the F- $\Delta$  response. The yield point is defined using the bolt elastic stiffness (Ke) and yield strength  $(F_v)$ . The ultimate point is determined by the ultimate plastic

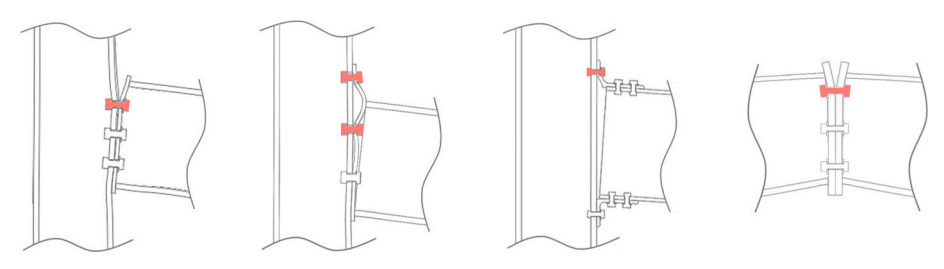
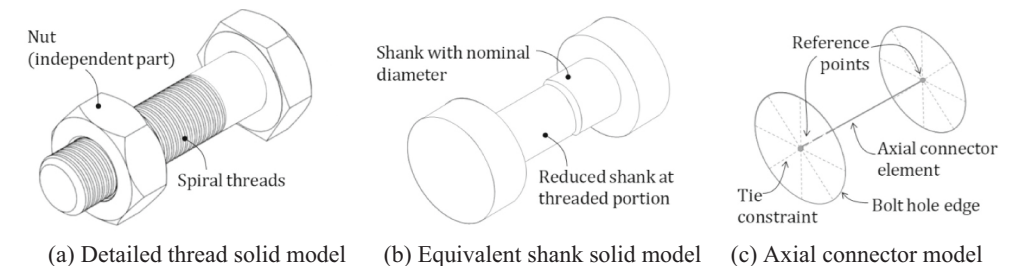


Fig. 1. Typical deformation modes in partial-strength bolted connections leading to bolt rupture.



- - Fig. 2. Typical bolt modeling techniques in CFE simulations.

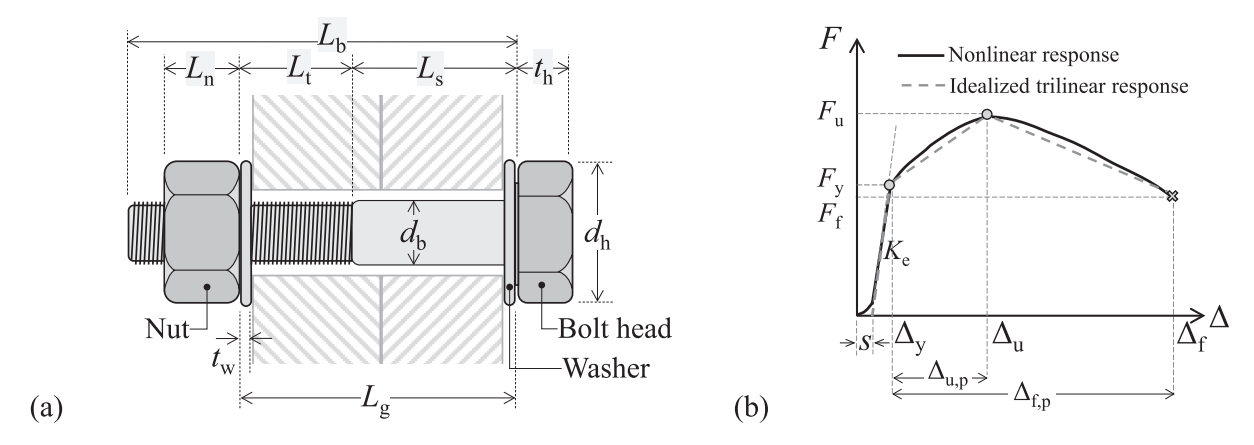


Fig. 3. (a) Bolt's main geometric parameters; (b) typical bolt tensile response and deduced parameters.

elongation  $(\Delta_{u,p})$  and the corresponding force  $(F_u).$  Note here that the ultimate plastic elongation is computed as the ultimate elongation  $(\Delta_u)$  minus the yield elongation. The failure point (i.e., post-necking behavior) is defined using the plastic elongation at complete failure  $(\Delta_{f,p})$  and the corresponding force  $(F_f)$ . These response parameters are quantified based on experimental data, as discussed in the following section.

## 3. Experimental dataset

# 3.1. Experimental study

A total of 200 HV-class high-strength bolts were tested. The bolts were either bright zinc-plated or galvanized and included both partial-thread and full-thread. Both grade 8.8 and 10.9 are considered as well as bolt sizes ranging from M12 to M24. Different bolt lengths were considered ranging from 75 mm to 150 mm. This is meant to vary the gripped thread length and investigate its effect (see supplementary data for the full test matrix).

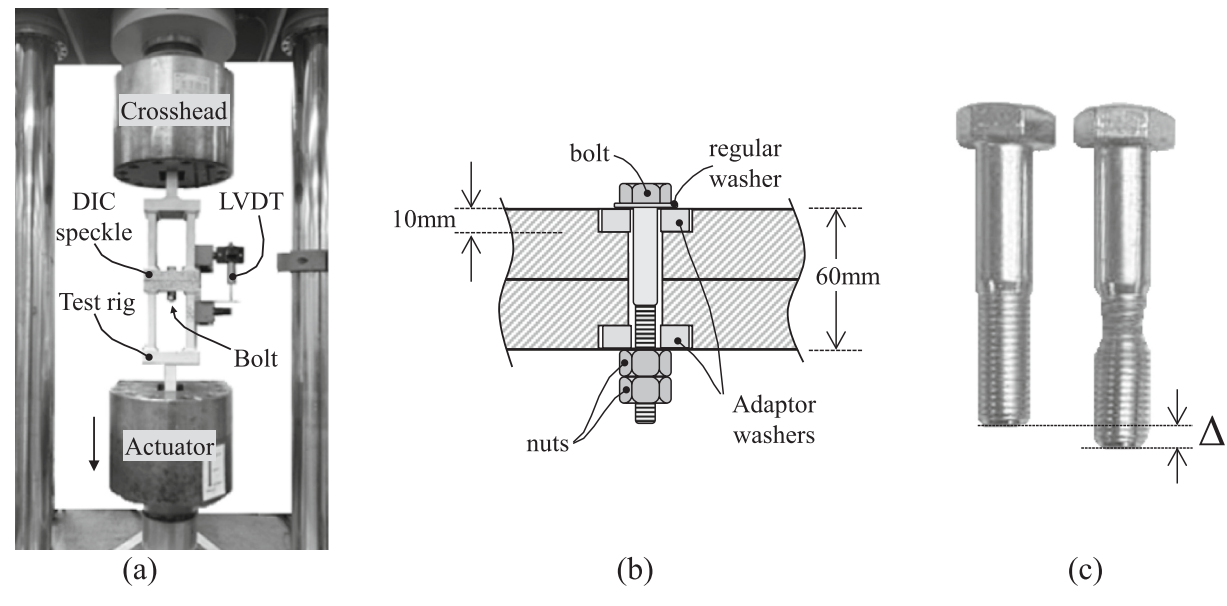


Fig. 4. Tensile bolt testing: (a) test setup; (b) test rig cross-section; (c) bolt axial elongation.

The bolt tests were conducted in the Testing and Structural Research Laboratory at the University of Southampton using a 630kN Schenck servo-hydraulic machine shown in Fig. 4(a). The bolt assembly is pulled using two identical rigid bolt rigs, each with a plate thickness of 30 mm. Hardened adaptor washers, inserted within groove holes in the rigs, are used to adapt the rig for different bolt sizes, as shown in Fig. 4(b). Those are 10 mm thick washers, fabricated from Grade EN24 steel, and have a + 1 mm larger hole diameter than that of the bolt (see Fig. 4(b)). In addition to the machine-recorded displacement, 2-dimensional Digital Image Correlation (DIC) and a redundant linear displacement potentiometer (LVDT) were used to track the planar movement of the test rig and the specimen. The test rig plates as well as the bolt head and nut were painted and speckled. This is done to measure the isolated bolt deformation, the test rig deformation, the separation distance between the rigid test rigs, and any potential slippage in the setup. Slippage between the machine grips and the test rigs was not observed in any test. Also, the test rig remained elastic in all tests. The levelness of the test rig plate and the verticality of the LVDT were checked using digital inclinometers before each test. The bolts were tightened to a snug-tight condition and then subjected to a tensile axial displacement at a constant loading speed of 0.05, 10, or 80 mm/s. The employed quasi-static speed of 0.05 mm/s is consistent with speeds used in past tests and conforms to the maximum speed limit as per ISO 898-1 [25] and ASTM 606/F606M-16 [5]. Two Grade 10.9 nuts were generally used in each test to eliminate the chance of thread stripping in the HV-type bolts. This was not possible however for the 75 mm long bolts where only one nut is used. Standard flat washers were sometimes used at the bolt head and/ or the nut to generate variations in the grip length. For a given bolt size and length, three identical tests are conducted to quantify response variability.

# 3.2. Overall failure modes and response characteristics

Fig. 5 shows example F- $\Delta$  responses of bolts with different grades and geometries. The displacement  $\Delta$  in these plots represents the isolated bolt's elongation without the setup's elastic deformations (see Fig. 4(c)), as tracked by the DIC system and confirmed by the redundant measurements. For the short 75 mm bolts with one nut (see Fig. 5(a)), thread stripping is observed as expected. The 100 mm long M16 bolts developed limited elongation with thread rupture occurring close to the shank as shown in Fig. 5(b) due to the short thread length within the gripped length ( $L_t$  less than 10 % of  $L_s$ ). Fig. 5(c) shows that bolts with lower grade and larger  $L_t$  develop larger elongation, as expected. These sample plots demonstrate the uncertainties in elastic stiffness, strength, and ductility (elongation capacity at failure) even when the bolts have the same geometric/material parameters and are produced by the same manufacturer. Those uncertainties are discussed and investigated in the next sections.

#### 3.3. Experimental dataset from the literature

Out of the 200 bolts tested herein, 108 were tested under quasi-static load. Those are complemented with 76 additional tests collected from ten other research programs in the literature, resulting in a dataset of 184 bolt specimens under quasi-static tensile load. Table 1 summarizes the main test parameters for the collected tests. Fig. 6 shows a breakdown of the dataset's basic parameters. In summary, most of the specimens are Gr 8.8 M16/M20 partially threaded bolts that failed by tensile rupture. The  $\emph{F-}\Delta$  response parameters are deduced and recorded for each test including the measured elastic stiffness ( $\emph{K}_e$ ), the measured critical plastic elongations (i.e.,  $\Delta_{u,p}$  and  $\Delta_{f,p}$ ), and the failure modes (e. g., stripping or rupture). Note that other researchers used comparable rigid test rigs. Nonetheless, the collected test data were carefully checked to ensure that the  $\emph{F-}\Delta$  curves reported by other researchers represent that of the bolt and exclude any elastic deformations from the test rig.

# 4. Proposed bolt's $F-\Delta$ model

In this section, the proposed model for defining each of the bolt's trilinear F- $\Delta$  parameters is discussed.

## 4.1. Initial elastic stiffness

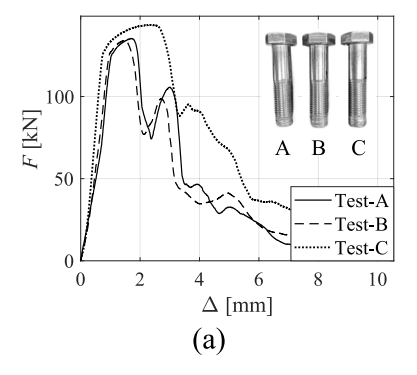
Computing the axial stiffness ( $K_e$ ) of a bolt assembly can be challenging due to the changing cross section and interaction between the nut and bolt's thread [13]. Few researchers provided analytical or hybrid analytical-empirical expressions for  $K_e$ . Agerskov [2] proposed an expression for computing the elastic deformation of non-preloaded bolts as given by Eq. (1), where  $n_w$  is the number of washers,  $t_w$  is the washer thickness, and  $A_{\text{nom}}$  is the bolt's nominal area. This expression considers the contributions of the shank, threads, washer, and nut. It was analytically driven and further modified by empirical coefficients. It was shown in the literature that this expression overestimates  $K_e$  by 9 % to 20 %, where larger errors are correlated with a shorter grip length [45].

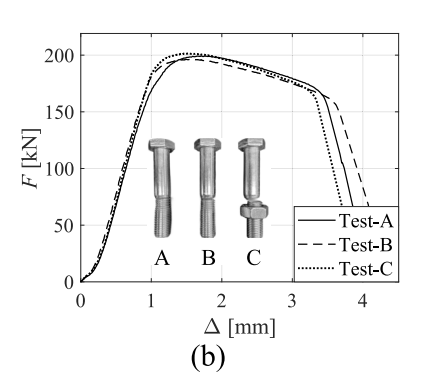
$$K_e = \frac{E A_{nom}}{(L_s + 1.43L_t + 0.71L_n) + 2(0.2L_n + 0.2 n_w t_w)}$$
(1)

Similarly, Swanson et al. [43] proposed Eq. (2), where  $\beta$  is a correction factor that was recommended to be taken equal to 0.55. Note, however, that earlier research [8,42] noted that  $\beta$  is not constant but rather varies from 0.3 to 2.86, indicating the large uncertainty for  $K_e$  computation. Consequently, it was observed that  $K_e$  predicted by this expression can be overestimated by 74 % in average [13].

$$\frac{1}{K_{\rm e}} = \frac{\beta d_{\rm b}}{E A_{\rm nom}} + \frac{L_{\rm s}}{E A_{\rm nom}} + \frac{L_{\rm t}}{E A_{\rm s}} + \frac{\beta d_{\rm b}}{E A_{\rm s}}$$
 (2)

The German standard VDI2230 [44] provides a code-based  $K_e$  model that considers the shank, threads, head, nut, and washer, as given in Eq.





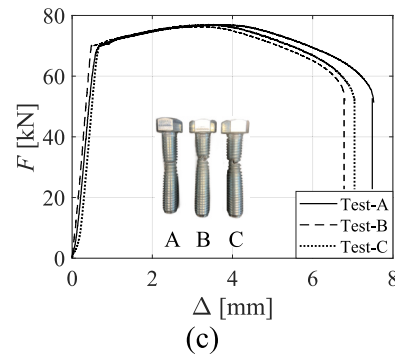


Fig. 5. Examples of bolt failure modes and F- $\Delta$  responses: (a) M16 Gr. 8.8  $L_b = 75$  mm; (b) M16 Gr. 10.9  $L_b = 100$  mm; (c) M12 Gr. 8.8  $L_b = 90$  mm.

**Table 1**Summary of the collected tests on high-strength bolt assemblies (quasi-static loading).

Reference	no.	Grade	d <sub>b</sub> [mm]	L <sub>b</sub> [mm]	L <sub>t</sub> [mm]	L <sub>s</sub> [mm]	L <sub>g</sub> [mm]
Authors' tests	108	8.8; 10.9	12;16;20;24	75–150	2.5-100	0–56	60–100
Hu et al. [24]	4	8.8	16	100	22.5	54	78
D'Aniello et al. [12]	11	10.9	16;20;24	100-120	7–24	56-73	80
Li et al. [29]	4	12.9	16;20;24	140	6-100	0-94	100
Li et al. [28]	4	10.9	16;20;24	140	5-100	0-95	100
Godrich et al. [20]	13	8.8; 10.9	16;20	105-161	4–99	0-109	84-144
Grimsmo et al. [21]	4	8.8	16	153	11-118	0-113	118-130
Schauwecker et al. [37]	4	10.9	10	_	5-60	0-55	60
Christopher et al. [11]	2	A490	22	_	3; 14	89	92; 103
Bendigo and Rumpf [7]	8	A325	22;25;29	_	51-102	0-115	102–171
Dlugosz and Fisher [15]	2	A325	22	_	3; 19	89; 105	108
Stranghoner et al. [41]	20	8.8; 10.9	16	100	20; 80	0; 60	80

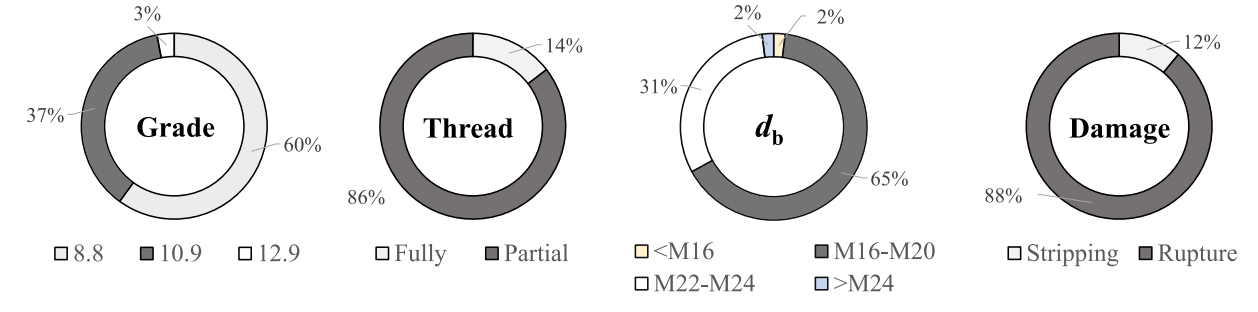


Fig. 6. Breakdown of the high-strength bolt database basic parameters.

(3), where  $d_{\rm h}$  is the bolt head diameter,  $d_{\rm w1}$  is the inner washer diameter, and  $d_{\rm w2}$  is the external washer diameter. Similarly, Eurocode 3 Part 1–8 [10] provides Eq. (4) to compute  $K_{\rm e}$  for a single bolt row (i.e., two bolts), as part of the component-based method, which considers the bolt head, shank, washer, and nuts.

$$\frac{1}{K_{\rm e}} = \frac{L_{\rm s} + 0.4 \ d_{\rm b}}{E \ A_{\rm nom}} + \frac{L_{\rm t} + 0.85 \ d_{\rm b}}{E \ A_{\rm s}} + \frac{n_{\rm w} \ t_{\rm w}}{E \ A_{\rm p}}$$

where, 
$$A_{p} = \frac{\pi}{4} \left( d_{h}^{2} - d_{w1}^{2} \right) + \frac{1}{2} \left( d_{w2}^{2} - d_{h}^{2} \right) \tan^{-1} \left[ \frac{0.75 \ d_{h} \ (n_{w} \ t_{w} - d_{h})}{\left( d_{w2}^{2} - d_{w1}^{2} \right)} \right]$$

$$(3)$$

$$K_{\rm e} = \frac{1.6 \, E \, A_{\rm s}}{L_{\rm g} + 0.5 \, t_{\rm h} + 0.5 \, L_{\rm n}} \tag{4}$$

The performance of these expressions is investigated against the experimental dataset (i.e., the 184 specimens discussed earlier). For this purpose,  $K_e$  is first deduced from the digitized F- $\Delta$  curves based on the secant slope joining the points at 20kN and 70 %  $F_u$ . This is a commonly used method [23] as it excludes any slippage/movement in the early

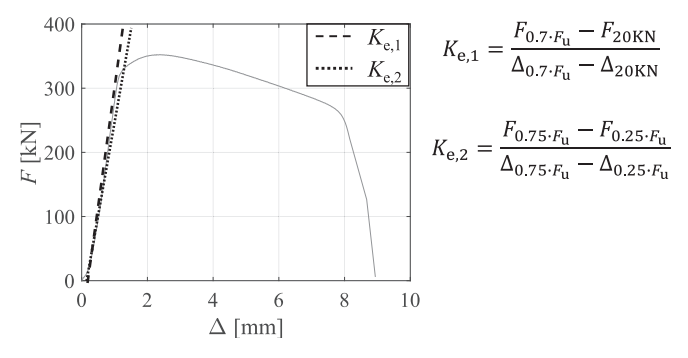


**Fig. 7.** Comparison between different  $K_e$  deduction methods.

stages of the F- $\Delta$  curve prior to the engagement of the bolt assembly components. Fig. 7 shows an example of  $K_e$  as deduced from the F- $\Delta$  curve (noted as  $K_{e,1}$  in the plot). In the same plot, to check the sensitivity of  $K_e$  deduction, another method is used to deduce  $K_e$  based on the 25 %  $F_u$  point rather than 20kN ( $K_{e,2}$ ). It is observed that the value of  $K_e$  can vary by up to 10 % depending on the deduction method with no observed bias with respect to one method or the other.

Fig. 8 shows the comparisons between the measured  $K_e$  and those predicted by the existing expressions. The expressions are evaluated assuming an average E=200 GPa. Note that changing the E value to 190 or 210 GPa would only shift the computed  $K_e$  values by  $\pm 5$  % which would not impact the assessment presented herein. It is observed that existing expressions do not provide consistently accurate estimates of the stiffness. All expressions, except for Eurocode 3, overestimate  $K_e$  by 50 % to 70 %, which is consistent with past observations in the literature [13,45]. The expression by Swanson et al. [43] can provide reasonable estimates if the  $\beta$  factor is taken equal to 2.5 (see Fig. 8(b)). The Eurocode expression mostly underestimates the bolt's stiffness by up to 50 %. Note that this expression does not consider the threaded region length.

To address the limitations of existing expressions, a more accurate one is developed herein. It is proposed to compute  $K_{\rm e}$  using a basic/simple analytical expression that is modified with a correction factor, as given by Eq. (5). The analytical stiffness ( $K_{\rm e,\ analytical}$ ) is based on the equivalent axial stiffness of the shank and the threaded portions within the griped region. The stiffness correction factor ( $\beta_{\rm k}$ ) is then computed as a function of  $d_{\rm b}$ ,  $L_{\rm g}$ ,  $L_{\rm t}$ , and  $L_{\rm n}$ , using the nonlinear power expression given in Eq. (6). The regression coefficients are regressed against the measured  $K_{\rm e}$  to  $K_{\rm e,\ analytical}$  ratios. The regression values corresponding to best fit (mean) as well as those based on the lower and upper bounds of the 68 % and 95 % prediction intervals are tabulated in Table 2. The fitted expression has an  $R^2$  of 0.70. As shown in Fig. 9, the new expression provides good  $K_{\rm e}$  estimates where 61 % and 95 % of the specimens are predicted with an error of less than 20 % and 50 %, respectively.

$$K_{e} = \beta_{k} K_{e,analytical} = \beta_{k} \frac{1}{\frac{L_{1}}{F_{A}} + \frac{L_{s}}{F_{A-res}}}$$

$$(5)$$

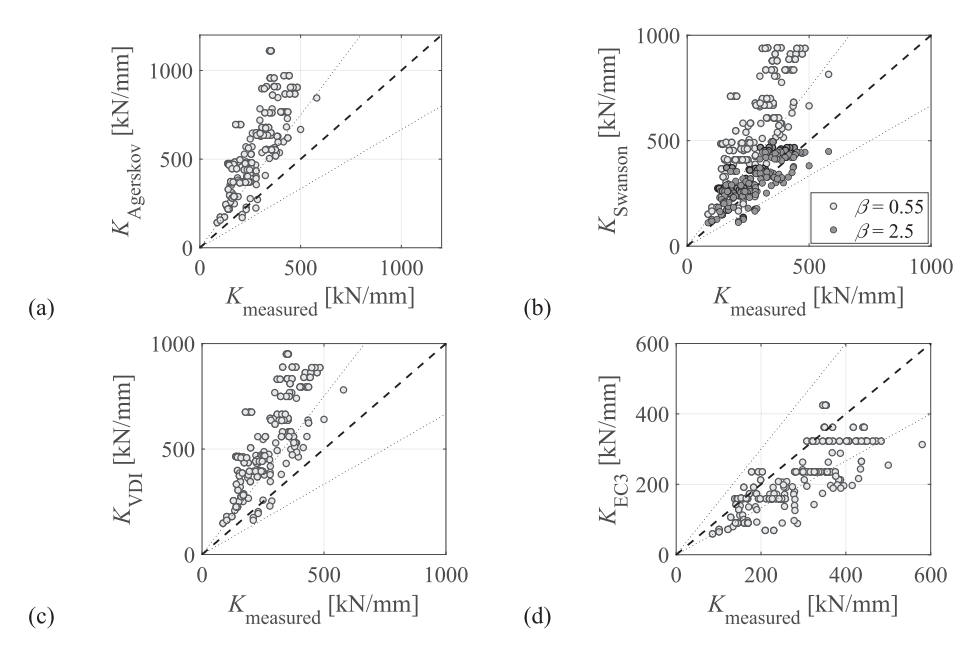


Fig. 8. Comparison between the measured  $K_e$  and existing predictive expressions: (a) Agerskov (1967); (b) Swanson et al. (2001); (c) VDI 2230; (d) Eurocode 3.

**Table 2** Regression coefficients for  $\beta_k$  based on data fitting and uncertainty bounds.\*

		•			
	Best fit	68 % PI		95 % PI	
	(mean)	LB	UB	LB	UB
$c_0$	0.362	0.338	0.387	0.316	0.415
$c_1$	-0.440	-0.430	-0.450	-0.420	-0.46
$c_2$	0.087	0.087	0.087	0.087	0.087
$c_3$	0.490	0.484	0.500	0.477	0.500
$c_4$	-0.320	-0.311	-0.330	-0.302	-0.340

PI: prediction interval, LB: lower bound, UB: upper bound.

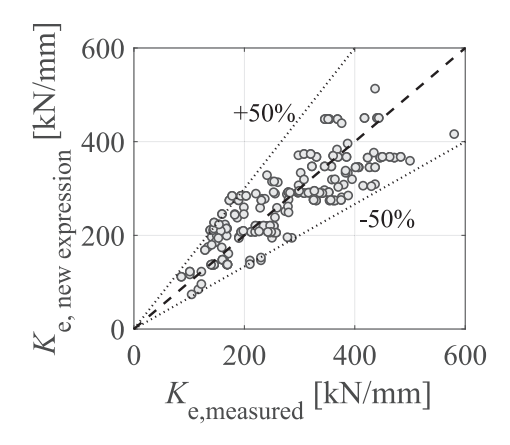


Fig. 9. Performance of the proposed  $K_{\rm e}$  expression.

$$\beta_{k} = c_{0} d_{b}^{c_{1}} L_{t}^{c_{2}} L_{g}^{c_{3}} L_{n}^{c_{4}} \text{ units} : [mm]$$
(6)

The previous  $K_e$  expression is meant to be utilized with the axial spring/connector approach. However, the need for the correction factor  $\beta_k$  to match bolt test data highlights an important issue that relates as well to CFE models that employ the equivalent shank solid model as illustrated earlier in Figure 2(b). In this model, only the shank and the threaded portions (within the gripped length) are represented. Therefore, the resulting axial stiffness is expected to be equivalent to  $K_e$ , analytical (which diverges from the true stiffness value). This is demonstrated in Fig. 10 where the result of a CFE simulation is compared with

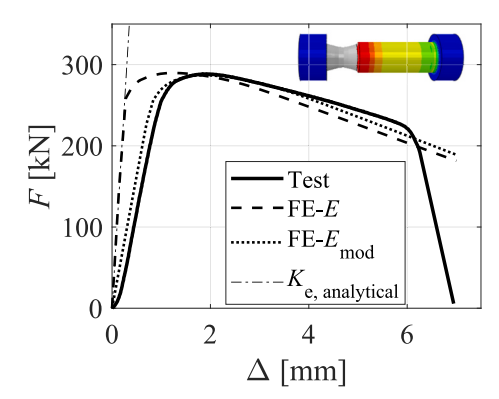


Fig. 10. Comparison between the equivalent shank solid model and test data considering modified modulus of elasticity.

test data for a sample specimen. The CFE simulation results in a much larger stiffness (~2 times larger). This is attributed to the exclusion of the threads from the current solid model. Consequently, the interaction between the threads of the nut and the bolt, and the resulting elastic deformations, are not captured. Note that the correct stiffness would be predicted if this interaction is explicitly captured, which is only feasible through the detailed thread solid model shown in Fig. 2(a). This issue was noted by D'Aniello et al. [13] where it was recommended to reduce the modulus of elasticity E by 50 % on average. A similar approach is employed here by modifying the modulus of elasticity using the  $\beta_k$  factor which considers the bolt's geometry, i.e.,  $E_{\text{mod}} = \beta_k E$ . When the bolt model is analyzed with the modified E, the stiffness matches the test data as shown in Fig. 10. It should be noted that for connections controlled by the deformations of other components, such as an endplate or an angle, this issue will have an insignificant impact on the joint stiffness. However, for other connections where the bolt is the weaker component, ignoring the E modification can result in erroneous global stiffness.

# 4.2. Yield and ultimate strengths

The bolt's yield and ultimate forces ( $F_y$  and  $F_u$ ) can be computed as the product of the bolt's tensile stress area ( $A_s$ ) and engineering yield and ultimate stresses ( $f_y$  and  $f_u$ ), respectively. For this purpose, the

strength parameters (i.e.,  $F_y$  and  $F_u$ ) are deduced from F- $\Delta$  curves. Specifically, the yield strength  $(F_y)$  is determined as the force at which the elastic slope diverges from the F- $\Delta$  curve, with respect to the elongation, by 10 % [16]. The ultimate strength  $(F_u)$  is directly determined when the F- $\Delta$  curve reaches the maximum point. Subsequently, the strength parameters are converted to the yield and ultimate stresses (i.e.,  $f_y$  and  $f_u$ ). Fig. 11 shows the histogram for the measured  $f_y$  and  $f_u$ / $f_y$  values for different bolt grades. The variability in the measured material stresses is evident in these distributions. Assuming they follow a normal distribution, the inherent material uncertainty is quantified using the 68 % prediction intervals (i.e.,  $\pm 1$  standard deviation,  $\sigma$ ) and superimposed in Fig. 11. In summary, coefficient of variations of 6.5 % and 3 % are observed on average for  $f_y$  and  $f_u$ / $f_y$ , respectively, which is consistent with past observations [31].

#### 4.3. Plastic ultimate and fracture elongations

The critical plastic elongations,  $\Delta_{u,p}$  and  $\Delta_{f,p}$ , are key to capturing the bolt's ductility. The critical elongations (i.e.,  $\Delta_u$  and  $\Delta_f$ ) are first deduced from the data and then transformed into the plastic elongations after subtracting the yield elongation as illustrated in Fig. 3(b). The relation between the plastic elongations and the gripped thread length ( $L_t$ ) is investigated in Fig. 12 while differentiating bolts by their grade (i.e., Gr 8.8/A325 and Gr 10.9/A490). It is observed that the critical plastic elongations linearly increase with  $L_t$ , as expected. The fitted linear functions are given by Eqs. (7) and (8). Note that for a bolt with a given grade and  $L_t$ , the critical plastic elongation may vary because of the inherent uncertainty associated with the material and the fracture phenomena. Therefore, the 68 % ( $\pm \sigma$ ) PIs are superimposed in the plots and summarized in Table 3. Those intervals can be used in sensitivity and reliability analysis or when conservative design is sought.

$$\Delta_{\rm u,p} = \begin{cases} 0.89 + 0.0360 \, L_{\rm t} \, {\rm Gr} \, 8.8 \\ 0.41 + 0.0357 \, L_{\rm t} \, {\rm Gr} \, 10.9 \end{cases} \tag{7}$$

$$\Delta_{\rm f,p} = \begin{cases} 5.82 + 0.0644 \, L_{\rm t} \, {\rm Gr} \, 8.8 \\ 2.87 + 0.0847 \, L_{\rm t} \, {\rm Gr} \, 10.9 \end{cases} \tag{7}$$

# 4.4. Maximum damage parameter

The post-ultimate drop in strength to  $F_{\rm f}$  can be represented using the maximum damage parameter ( $D_{\rm max}$ ) which is defined as 1- $F_{\rm f}/F_{\rm u}$ . Based on the collected data, Fig. 13(a) shows the distribution of  $D_{\rm max}$ , which

has an average value of 0.32 and a standard deviation of 0.05. Fig. 13(b) shows the QQ plot of the  $D_{\rm max}$  distribution with a linear correlation. Note that the p-value is computed as 0.39, which indicates the  $D_{\rm max}$  is normally distributed regardless of the material and geometric parameters.

#### 4.5. Procedures for constructing a bolt spring model

To construct the trilinear connector model, the following steps are recommended:

- 1) Using the bolt's geometric parameters ( $d_b$ ,  $L_g$ ,  $L_t$ , and  $L_n$ ), compute the elastic analytical stiffness ( $K_{\rm e,\ analytical}$ ) using Eq. (5).
- 2) Modify  $K_e$  using the correction factor ( $\beta_k$ ) as per Eq. (6).
- 3) Compute the plastic ultimate and failure elongations ( $\Delta_{u,p}$  and  $\Delta_{f,p}$ ) using Eqns. (7) and (8), respectively.
- 4) Compute the bolt's yield and ultimate forces ( $F_y$  and  $F_u$ ) as the product of the bolt's tensile stress area ( $A_s$ ) and yield and ultimate stresses ( $f_y$  and  $f_u$ ), respectively. The stress values can be assumed as the nominal or the expected ones based on the statistical metrics summarized in Figure 11. Alternatively, other material variability factors from the literature can be used [31].
- 5) Lastly, assume a value for  $D_{\text{max}}$  based on the distribution in Fig. 13 and use it to compute the failure force ( $F_f = D_{\text{max}} F_u$ ).

One should note that the constructed F- $\Delta$  response excludes the initial deformation phase, noted by "s" in Fig. 3(b). This phase is about 0.2 mm on average and is associated with low stiffness at low load levels. This primarily occurs due to thread engagement slack, surface irregularities, or when the bolts are not fully-pretensioned [24]. For practical purposes concerned with joint- and system-level responses, this phase has no impact.

#### 5. Validation of the proposed model

In this section, the accuracy of the proposed methodology for simulating bolt fracture is examined in comparison with several past test specimens. The section is divided into two subsections. First, the methodology is validated against isolated bolt assemblies in tension. Second, the methodology is validated against full-scale beam-to-column joints with endplate connections under monotonic joint rotation.

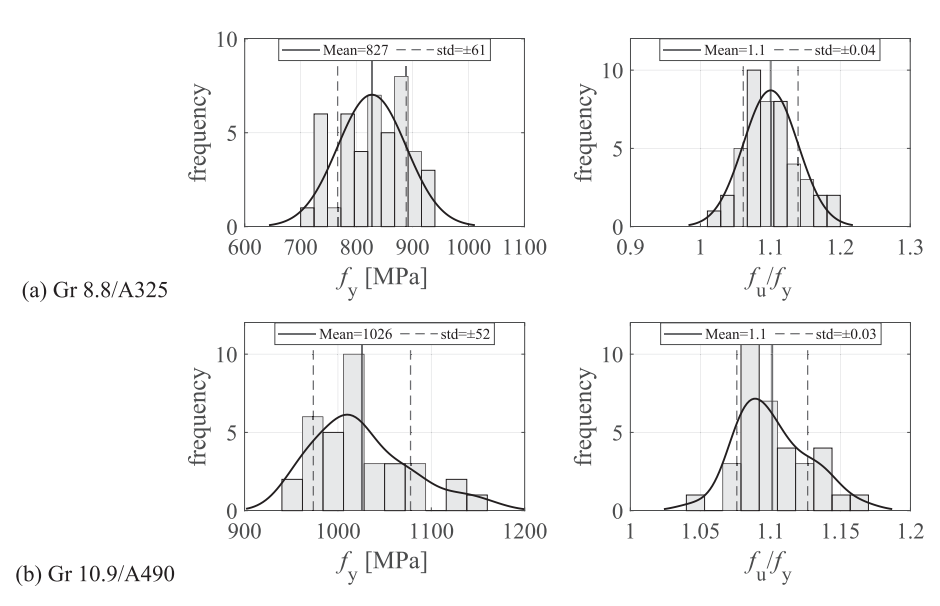


Fig. 11. Distribution of the bolt's measured engineering stress parameters based on the collected dataset.

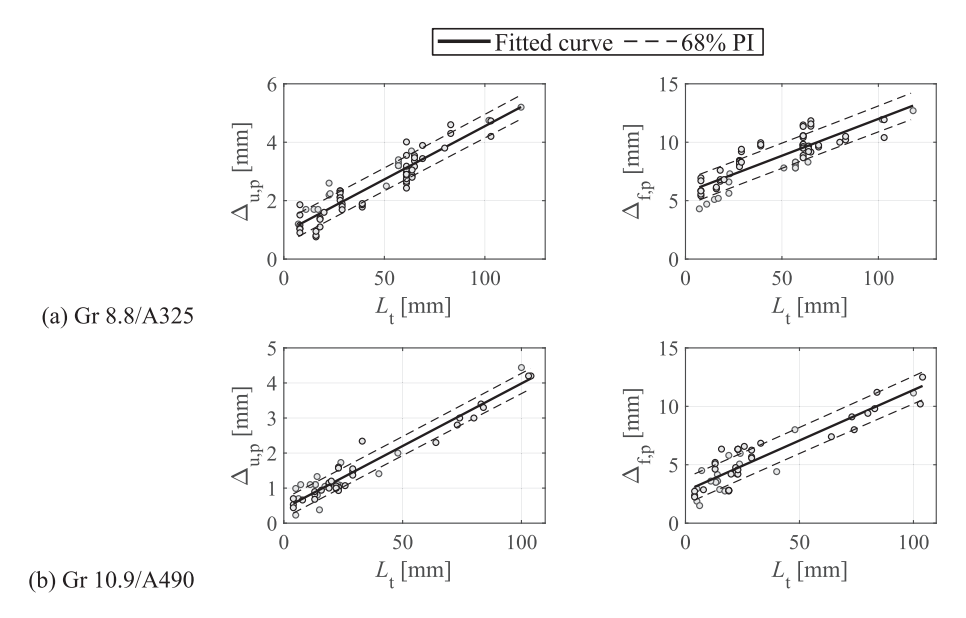


Fig. 12. Established relations between the ultimate and fracture plastic elongations and the gripped thread length.

**Table 3**Uncertainty bounds for carbon steel bolts' critical plastic elongations.

Grade	68 % PI		95 % PI	
	$\Delta_{\mathrm{u,p}}$ [mm]	$\Delta_{f,p}$ [mm]	$\Delta_{\mathrm{u,p}}$ [mm]	$\Delta_{f,p}$ [mm]
8.8	Eq. (7) $\pm$ 0.43	Eq. (8) $\pm$ 1.1	Eq. (7) $\pm$ 0.85	Eq. (8) $\pm$ 2.2
10.9	Eq. (7) $\pm$ 0.30	Eq. (8) $\pm$ 1.2	Eq. (7) $\pm$ 0.60	Eq. (8) $\pm$ 2.4

# 5.1. Bolt assembly tests

(a)

In this section, validation is conducted against four carbon steel bolt assemblies from four different experimental studies [12,21,24,28]. The grade and geometric details of the validation bolt specimens are summarized in Table 4. All the specimens experienced necking followed by rupture within the threaded area. Fig. 14 shows comparisons of the F- $\Delta$  test curves and those predicted by the empirical connector model. In these plots, the predicted responses are based on the mean and 68 % upper and lower PI bounds. The shaded area between the 68 % PI lines represents the uncertainty range for the prediction. For all cases, damage initiation (at  $F_{\rm u}$ ) is well predicted, the damage evolution (post-peak degrading –negative- slope) is in good agreement with the test data, and the observed bolt failure elongation  $\Delta_{\rm f}$  (at complete loss of force) falls within the 68 % PI bounds. Apart from the ductility, the equivalent elastic stiffnesses computed by Eq. (5), as well as the strength values, for all assemblies also show a good agreement with the test data.

#### 5.2. Joint tests

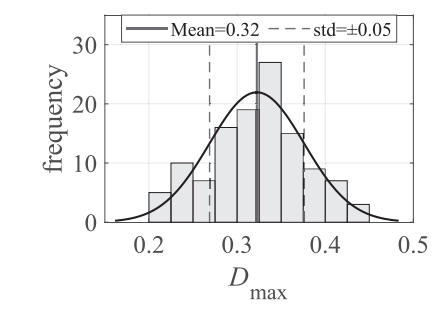
Five full-scale joint specimens with extended and flush endplate connections are selected from five different research studies [32–35,38] for validation. These specimens have different geometry, bolt sizes, and material properties, as summarized in Table 5. All specimens were subjected to ramped monotonic loading and eventually failed by bolt rupture. Bolt rupture was preceded by visible plastic deformations in the various connection components (column flange bending, panel zone in shear, beam buckling, endplate bending, bolt elongation, etc.).

The CFE models are developed within the commercial software Abaqus/CAE [1]. Boundary conditions, representative of each test setup, were applied. The boundary conditions were applied to reference points allocated at the centers of the column and beam(s) ends. Each reference point is connected using a rigid body constraint to the column or beam end surface. A global interaction property is defined to characterize the contact between the different model parts. This included hard contact

**Table 4**Summary of the validated bolt assemblies, their geometry, and the calculated mean response parameters [unit: mm and kN/mm].

Reference	Bolt*	Grade	$L_{\mathrm{g}}$	$L_{t}$	$\Delta_{\mathrm{u,p}}$	$\Delta_{f,p}$	$K_{\mathrm{e}}$
Grimsmo et al. [21]	M16 PT	8.8	130	17	1.5	6.9	196
D'Aniello et al.[12]	M24 PT	10.9	80	23	1.2	4.8	413
Li et al. [28]	M20 FT	10.9	100	100	4.0	11.3	292
Hu et al. [24]	M20 PT	8.8	77.5	22.5	1.7	6.3	337

<sup>\*</sup> PT: partially threaded; FT: fully threaded.



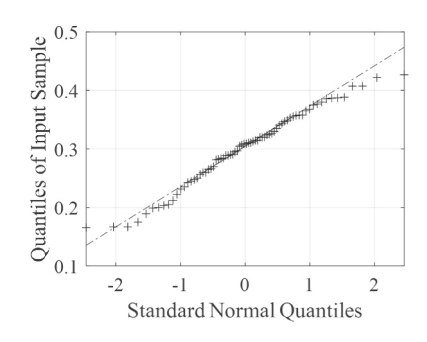


Fig. 13. Maximum damage parameter  $D_{\text{max}}$ : (a) histogram with fitted normal distribution; (b) QQ plot.

(b)

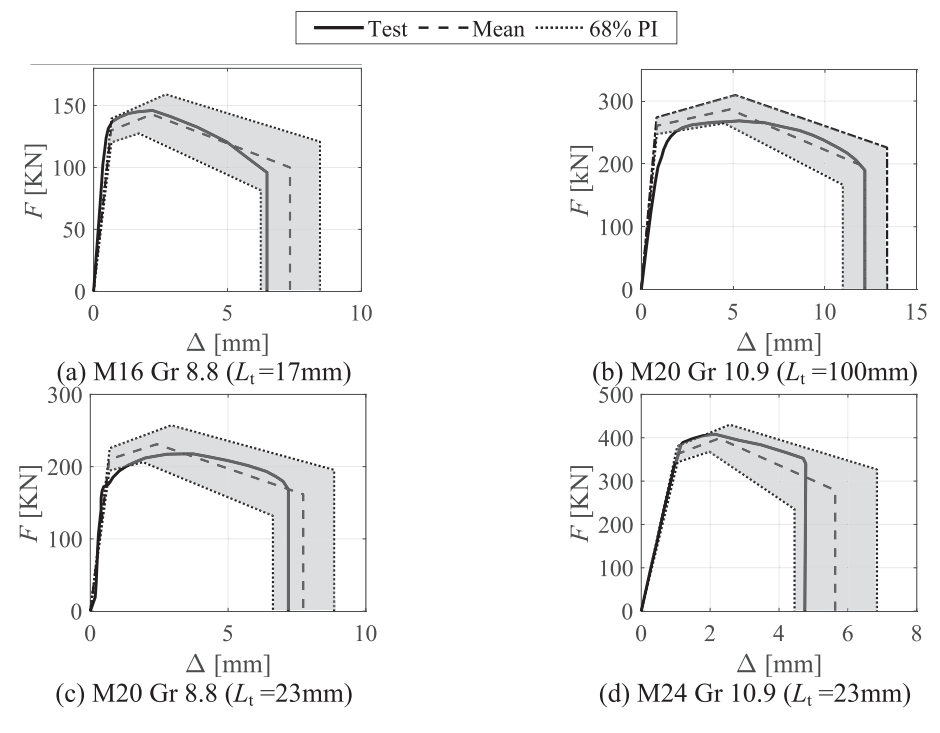


Fig. 14. Comparison of F- $\Delta$  response for different bolt assemblies demonstrating uncertainty range.

**Table 5**Summary of the validated full-scale joint specimens' main attributes.

Reference	ID	Туре	Column	Beam	t <sub>ep</sub> [mm]	Bolt
Munter et al. [32]	Test2	Splice Extended	_	IPE 400	14	M20 10.9
Qiang et al. [34]	2-3 A	Exterior Flush	HW 400x400x284	HW 300x300x95	15	M27 8.8
Rolle [35]	S6	Interior Flush	HEB 300	IPE 500	12	M20 10.9
Shi et al. [38]	JD3-M	Exterior Extended	BU 300x250x8x12*	BU 300x250x8x12	20	M20 10.9
Nogueiro [33]	J4-1	Exterior Extended	HEA 320*	HEA 280	18	M24 10.9

<sup>\*</sup> Stiffened column flanges.

(in compression), allowed separation after contact, and a friction coefficient of 0.3. Surface-to-surface tie constraint is applied between the beam-endplate and stiffener-column interfaces (if applicable) instead of the weld. All components, except for the bolt, were meshed with quadratic tetrahedron elements (C3D10M) with a mesh size ranging between 10 mm to 20 mm. For the endplate, two elements were used through the thickness. The components' elastic and plastic behaviors are defined based on the reported material stress-strain values, as summarized in Table 6. The plastic behavior is based on the Von Mises yield criteria with isotropic hardening and is defined up to the necking point (i.e., post-necking behavior is perfectly plastic). The trilinear bolt models are summarized in Table 7. Note that the axial connector detail is shown in Fig. 15(a) where two reference points were applied to couple the internal surfaces of the bolt head and nut. It is recommended that the bolt head and nut are modeled using solid elements such that yield line patterns in the connected elements are correctly captured. The connector stiffness and ductility parameters were computed. The connector is assigned an axial property where elastic, plastic (post-yield branch), and damage (post-ultimate branch) properties are defined -blindly- based on the previously outlined procedure. The dynamic Explicit solver is used while maintaining a slow loading rate, consistent with the validated quasi-static tests, with insignificant inertia forces and low kinetic energy maintained.

Fig. 15(b-f) shows comparisons of the moment-rotation response between the test data and computational simulations. In these plots, the CFE simulation results are shown up to the point of the first bolt rupture occurrence (noted here as the failure rotation,  $\theta_f$ ); subsequent bolt

 Table 6

 Material properties of validation joint specimens' components.

Reference	Specimen	Component	Grade	E [MPa]	f <sub>y</sub> [MPa]	f <sub>u</sub> [MPa]
Munter et al.	Test2	Beam Endplate	Fe360	200,000 200,000	300 312	450 456
[32]	10002	Bolt	Gr 10.9	200,000	990	1100
Qiang et al.	2-3 A	Column/ Beam	Q345	185,550	356	550
	2-3 A	Endplate	S690	185,550	789	820
[34]		Bolt	Gr 8.8	199,167	700	950
		All	S355	200,000	379	537
Rolle [35]	S6	Bolt	Gr 10.9	200,000	990	1133
		Column		192,061	409	537
Shi et al.		Beam	Q345	195,452	409	537
	JD3-M	Endplate		188,671	409	537
[38]		Bolt	Gr 10.9	206,000	995	1161
Nonucius		Column/ Beam	S355	207,900	461	580
Nogueiro [33]	J4-1	Endplate		209,000	415	540
[33]		Bolt	Gr 10.9	213,000	990	1170

**Table 7**Computed damage parameters for the bolt components in the connector.

Reference	Specimen	Bolt	L <sub>t</sub> [mm]	$\Delta_{\mathrm{u,p,mean}}$ [mm]	$\Delta_{ m f,p,mean} \ [ m mm]$
Munter et al. [32]	Test2	M20 (FT)	28	1.40	5.20
Qiang et al. [34]	2-3 A	M27 (FT)	50	2.70	9.00
Rolle [35]	S6	M20 (PT)	16	0.98	4.20
Shi et al. [38]	JD3-M	M20 (PT)	10	0.77	3.70
Nogueiro [33]	J4–1	M24 (PT)	10	0.77	3.70

failures, that would drop the moment capacity to zero, are omitted. The computational simulation shows a good agreement with the test data. Some differences in the initial stiffness and maximum strength of the connection are observed in the joint specimens; however, this difference does not exceed 15 %. The priority of the current study is to examine the validity of the proposed methodology in reasonably predicting the failure rotation of actual joints. As such, tuning the computational model parameters to achieve a perfect fit with the moment-rotation test data was not a priority. Note that the error in the mean predicted failure rotation of all specimens (i.e., based on the bolt's mean critical elongations as per Eqs. (7) and (8)) is within  $\pm 10$  %, as summarized in Table 8, which is acceptable from the perspective of engineering practice. Most importantly, the predicted failure rotation of all specimens fell

within the 68 % PI bounds with a maximum error range of about  $\pm 20$  %. Referring to Table 8. the 68 % PI uncertainty in bolt ductility can result in up to  $\pm 1.3$  % rads variation in the joint's rotational ductility. Note that a larger variation would be observed if the 95 % PI bounds are employed. In summary, these validations demonstrate the ability of the proposed model to capture bolt failure within a real scenario where the bolt is subjected to combined actions (i.e., the stress state deviates from pure uniaxial tension). This is particularly notable considering that the computational models involved blind application of the methodology without any material calibration or model tuning.

# 6. Implications of the loading speed on bolt response

Actual hazards (e.g., earthquake, explosion, or sudden column loss) induce faster loading speeds on the joint components including the bolts. Past tests mostly investigated the strain-rate-dependent properties of the bolt material using round (i.e., turned-down) coupon specimens. Grimsmo et al. [22] tested Gr 8.8 coupons under different strain rates (i. e., from  $10^{-3}$  to  $10^2$  s<sup>-1</sup>). It was observed that the ultimate stress ( $f_u$ ) can increase by up to 15 %, while the fracture strain showed no clear dependency. Similarly, Kendall et al. [27] observed that the ultimate strain was slightly increased, whereas the fracture strain remained constant for Gr 8.8 material under a loading speed of 0.05 to 10 mm/s. Yang et al. [47] tested Gr 8.8 and 12.9 coupons with strain rates ranging from 0.00025 to 100 s<sup>-1</sup> and observed that the strength increased by up to 15%, the ultimate strains increased by 35%, and the fracture strain was non-correlated to strain rates. Studies on bolt assembly behavior under high-speed loading are still limited. Therefore, a series of tests were

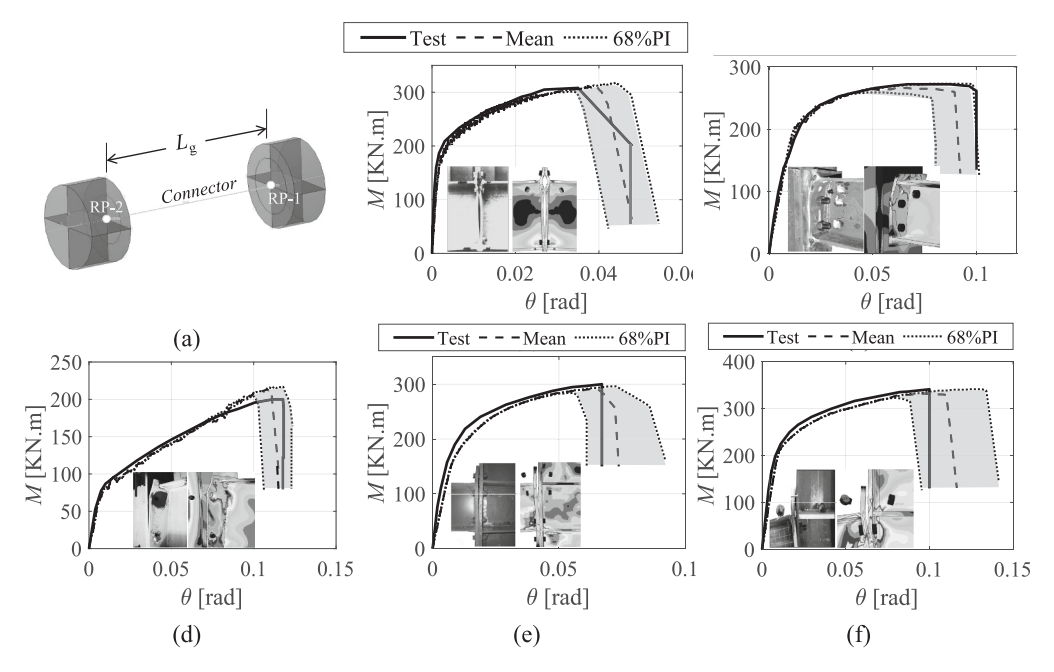


Fig. 15. Validation of the proposed methodology against full-scale bolted endplate joints.

**Table 8**Range of observed errors in precited failure rotation based on full-scale joint tests.\*

Reference	Specimen	$\theta_{ m f,test}$ [rad]	θ <sub>f, CFE</sub> [% r	$ heta_{ extsf{f},  ext{ CFE}}$ [% rads]			Relative error [%]		
			LB	M	UB	LB	M	UB	
Munter et al. [32]	Test2	0.035	3.2	3.8	4.4	-8.6	8.6	25	
Qiang et al. [34]	2-3 A	0.100	7.9	9.0	10.0	-20	-10	0	
Rolle [35]	S6	0.118	10.0	11.0	12.0	-15	-7	1.6	
Shi et al. [38]	JD3-M	0.067	5.6	6.5	7.6	-16	-3	13	
Nogueiro [33]	J4-1	0.100	8.9	10.3	11.6	-11	3	16	

<sup>\*</sup> Lower boundary (LB), mean value (M), and upper boundary (UB).

conducted as part of this experimental campaign to further investigate this issue

Out of the 200 specimens, 92 were tested under high-speed loading: 56 bolts were tested at 10 mm/s and 35 bolts at 80 mm/s. Those two speeds are equivalent to strain rates of about 0.5 to 8 s $^{-1}$  (assuming a gauge length of 10 mm). Fig. 16(a) shows a sample plot of a bolt assembly under different loading speeds. Note that for 10 mm/s tests, the actual speed reached the target speed before the yield point as demonstrated in Fig. 16(b) while for the 80 mm/s tests, the speed at the yield point was slightly less ( $\sim$  76 mm/s).

The bolt response parameters are deduced from the dynamic (i.e., 10 and 80 mm/s) force-elongation curves and normalized by the corresponding values of the quasi-static tests (i.e., 0.05 mm/s). Fig. 17 shows the average normalized dynamic responses for strength and ductility. Overall, the strength ( $f_v$  and  $f_u$ ) and plastic ultimate elongation ( $\Delta_{u,p}$ ) visually show an increase with the increase in loading speed, whereas no clear dependency is observed in the plastic fracture elongation ( $\Delta_{u,f}$ ). Those observations are consistent with the previous tests [22,47]. To quantify the loading speed effect, Table 9 summarizes the factors of the normalized responses (i.e., dynamic-to-static ratios). Concerning strength ( $f_v$  and  $f_u$ ), both Gr 8.8 and 10.9 bolts develop a 1 % increase for  $f_{\rm v}$  at 10 mm/s. While larger increases are observed at 80 mm/s, which are 6 % and 4 % for Gr 8.8 and 10.9 bolts, respectively. Similar dependency is observed in  $f_u$ , a 2 % increase is observed for both Gr 8.8 and 10.9 bolts at 10 mm/s. When it comes to 80 mm/s, Gr 8.8 and 10.9 bolts develop an increase of around 4 %. For ductility ( $\Delta_{u,p}$  and  $\Delta_{u,f}$ ), both Gr 8.8 and 10.9 bolts show an increase with the increase of loading rate for  $\Delta_{\text{u.p.}}$  Specifically, an increase of up to 10 % was observed at 80 mm/s regardless of bolt grades. When it comes to 10 mm/s, Gr 8.8 and 10.9 bolts develop an increase of 4 % and 8 % for Gr 8.8 and 10.9 bolts, respectively. Finally, Gr 8.8 and 10.9 bolts show an over 5 % decrease in  $\Delta_{u,f}$  at 10 mm/s, whereas the  $\Delta_{u,f}$  at 80 mm/s is slightly decreased by 3 % and increased by 1 % for Gr 8.8 and 10.9 bolts, respectively.

# 7. Model limitations

The developed model and empirical expressions are valid for partial- and full-threaded bolts of grade 8.8, A325, 10.9, or A490 with a nominal diameter between 12 mm and 30 mm and a grip length between 60 mm and 170 mm. Those ranges cover the ones allowed in construction practice EN-15048 [19]. The model can be potentially extrapolated to long structural rods/bolts ( $L_{\rm g} > 200$  mm). Note however that for steel rods that are cold-forged (not heat-treated), the post-ultimate plastic elongation may be omitted [26].

In joints undergoing rotational demands, the bolts are subjected to combined tension and shear. The bolt's shear to tension force ratio depends on several factors such as the number of bolts, the beam length, gravity loads, catenary action, and level of rotation. Based on a recently compiled database for full-scale joint tests [4,9], when the connection reaches its capacity, the ratio of shear to tension force in bolts as part of flush and extended endplate connections varies between 0.01 and 0.2 with an average value of 0.07. This level of shear force is not detrimental to the bolt behavior ([5,29,40,41]). Accordingly, the proposed model is

(a)

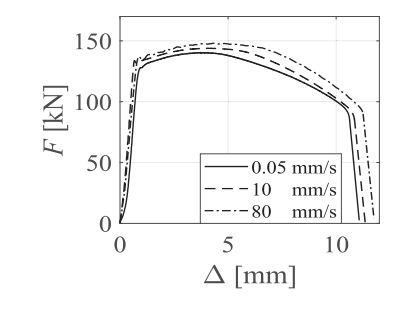
valid for such cases. Conversely, for connections where the bolts are under dominant shear or bearing stresses, such as shear-tab or double web-angle connections, the model is not appropriate.

The loading speed (strain rate) effect is assessed herein based on 92 tests at two loading speeds. Accordingly, the assessment is done in a rather qualitative manner while evaluating the average change in the bolt's response quantities under higher loading speeds. Considering the observed relatively strong variability in the test results at high loading speeds, much more data is needed (across a wider range of varying loading speeds) to capture the underlying response correlations/dependencies and to potentially develop explicit expressions that consider the loading speed. Until then, the connection response can be potentially evaluated at high loading speeds using the developed quasi-static expressions, after being modified using the quantified dynamic-to-static ratios.

# 8. Summary and conclusions

Bolt tensile rupture is a fundamental failure mode in bolted steel joints, particularly those with semi-rigid connections. There is a growing interest in quantifying the ductility of such connections with accuracy. As part of performance-based design and assessment of structures, it is important to quantify this while considering uncertainty. Toward that goal, work was undertaken to develop an empirical spring model for simulating the response of high-strength steel bolts undergoing tension for use in practical applications utilizing continuum finite element (CFE) or mechanical (component-based) models. The work's highlights and main conclusions are as follows:

- A parametric experimental study was conducted on 200 highstrength carbon steel bolt assemblies with varying sizes, lengths, grades, coating, and loading speeds. The data is complemented with 76 similar tests collected from the literature to create a multiattribute experimental dataset covering a wide range of European/ American bolt grades and geometric properties.
- Existing research- and code-based analytical/empirical expressions
  for estimating the elastic axial stiffness of high-strength bolts were
  assessed against the dataset. These expressions were found to be
  inconsistent in accuracy, sometimes resulting in errors of up to ±2
  times the expected value. This is because the elastic interaction between the nut and the bolt threads is not being captured.
- Utilizing the experimental dataset, an expression was developed to predict the bolt's elastic axial stiffness. The expression is a basic analytical one that represents the equivalent bolt stiffness considering the shank and threaded portions within the gripped length. This analytical expression is modified by a correction factor  $(\beta_k)$  that is empirically computed as a function of the bolt's diameter, grip length, thread length, and the length covered by the nut(s).
- Utilizing the experimental dataset, empirical expressions are established relating the bolt's critical plastic elongations with its grade and gripped thread length. The uncertainty associated with the bolt's elongation at fracture is shown to have a coefficient of variation of



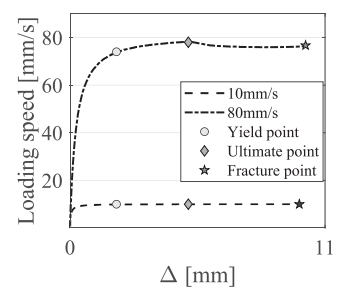


Fig. 16. Bolt responses under high-speed loading: (a) force-elongation responses; (b) speed evolution as a function of bolt elongation.

(b)

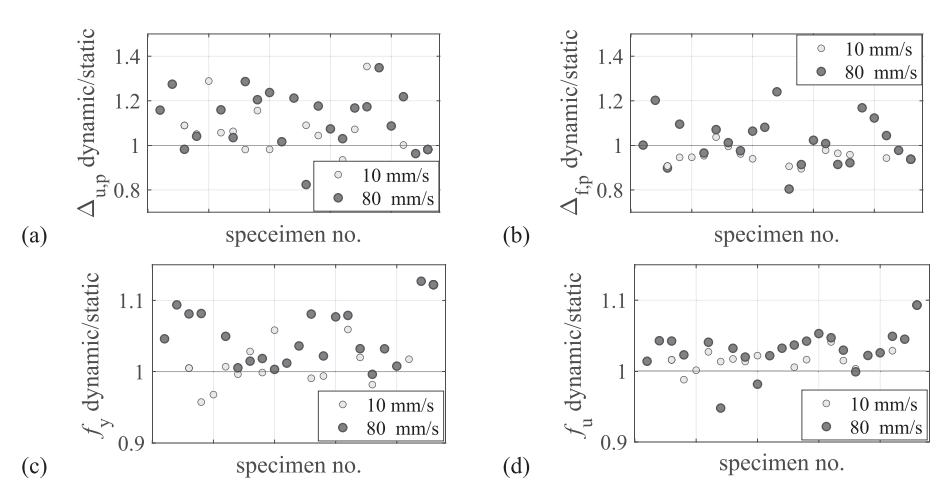


Fig. 17. Dynamic-to-static response ratios for bolt assemblies under different loading speeds.

**Table 9**Summary of average dynamic-to-static ratios for the plastic elongation and stress parameters.

	Loading speed [mm/s]	Average	dynamic-t	o-static rati	0
		$\Delta_{\mathrm{u,p}}$	$\Delta_{f,p}$	$f_{\mathrm{y}}$	$f_{ m u}$
000	10	1.04	0.92	1.01	1.02
Gr 8.8	80	1.10	0.97	1.06	1.03
C= 10.0	10	1.08	0.94	1.01	1.02
Gr 10.9	80	1.10	1.01	f <sub>y</sub> 1.01 1.06	1.04

about 20 %. This uncertainty can translate to up to a notable  $\pm 1.3$  % rads variation in the rotational ductility at the joint level.

- The percentage drop in the bolt's ultimate strength before complete fracture is found to be about 32 % with a standard deviation of 5 %.
- Faster loading rates can affect the bolt's response, especially for strength and ductility. The strengths  $f_y$  and  $f_u$  are amplified on average by 5 % and 4 % for Gr 8.8 and 10.9 bolts, respectively. With respect to ductility, the change in the ultimate plastic elongation ( $\Delta_u$ ,  $_p$ ) can reach to 10 % on average at 80 mm/s. Consistent with past research, no clear dependency is observed for the plastic elongation at fracture ( $\Delta_{f,p}$ ) where it may be amplified or reduced by 20 % at 80 mm/s.

Supplementary data to this article can be found online at https://doi.org/10.1016/j.jcsr.2025.109574.

# CRediT authorship contribution statement

**Zizhou Ding:** Writing – original draft, Visualization, Validation, Investigation, Formal analysis, Data curation. **Ahmed Elkady:** Writing – review & editing, Supervision, Methodology, Funding acquisition, Conceptualization.

# Declaration of competing interest

The authors declare that they have no known competing financial interests or personal relationships that could have appeared to influence the work reported in this paper.

# Acknowledgments

This work was conducted at the National Infrastructure Laboratory, University of Southampton (UoS). The authors gratefully acknowledge the financial support provided by UoS to the first author as part of their studentship. The authors would like to thank the Testing and Structures

Research Laboratory (TSRL) staff for their technical assistance throughout the testing program.

#### Data availability

The experimental dataset upon which the current work is based is provided in the paper's the supplementary material. The proposed trilinear model is also provided through a graphical user-interface tool that is downloadable from GitHub [17]. Further data can be made available from the corresponding author upon reasonable request.

#### References

- [1] Dassault Systemes Simulia Corp., RI, USA, © Dassault Systèmes, 2010.
- [2] H. Agerskov, High-strength bolted connections subject to prying, J. Struct. Div. 102 (1) (1976) 161–175, https://doi.org/10.1061/JSDEAG.0004253.
- [3] AISC, Specifications for Structural Steel Buildings. Ansi/aisc360-10, American Institute of Steel Construction (AISC), Chicago, 2022.
- [4] H. Akiyama, Evaluation of fractural mode of failure in steel structures following Kobe lessons, J. Constr. Steel Res. 55 (1–3) (2000) 211–227, https://doi.org/ 10.1016/S0143-974X(99)00086-3.
- [5] ASTM, Standard Test Methods for Determining the Mechanical Properties of Externally and Internally Threaded Fasteners, Washers, Direct Tension Indicators, and Rivets, American Society for Testing and Materials, West Conshohocken, PA, 2016.
- [6] M. Bahrami, Behaviour of Beam-to-Column End Plate Connections in Structural Steelwork, Ph.D. Thesis, Dundee Institute of Technology, Scotaland, UK, 1991.
- [7] R.A. Bendigo, J.L. Rumpf, Calibration and Installation of High Strength Bolts, Fritz Engineering Laboratory, Department of Civil Engineering, Lehigh University, 1959.
- [8] J. Bickford, Handbook of Bolts and Bolted Joints, MarcelDekker, 1998.
- [9] B. Bose, J.K. Youngson, Z.M. Wang, An appraisal of the design rules in eurocode 3 for bolted end-plate joints by comparison with experimental results, Proc. Inst. Civ. Eng.: Struct. Build. 116 (2) (1996) 221–234, https://doi.org/10.1680/ istbu.1996.28289.
- [10] CEN, Eurocode 3 Design of Steel Structures, Part 1–8: Design of Joints, European Committee for Standardization, Brussels, Belgium, 2005.
- [11] R.J. Christopher, G.L. Kulak, J.W. Fisher, Calibration of alloy steel bolts, J. Struct. Div. 92 (2) (1966) 19–40, https://doi.org/10.1061/JSDEAG.0001419.
- [12] M. D'Aniello, D. Cassiano, R. Landolfo, Monotonic and cyclic inelastic tensile response of european preloadable gr10. 9 bolt assemblies, J. Constr. Steel Res. 124 (2016) 77–90, https://doi.org/10.1016/j.jcsr.2016.05.017.
- [13] M. D'Aniello, D. Cassiano, R. Landolfo, Simplified criteria for finite element modelling of european preloadable bolts, Steel Compos. Struct. 24 (6) (2017) 643–658, https://doi.org/10.12989/scs.2017.24.6.643.
- [14] Z. Ding, A. Elkady, Semirigid bolted endplate moment connections: review and experimental-based assessment of available predictive models, J. Struct. Eng. 149 (9) (2023) 04023117, https://doi.org/10.1061/JSENDH.STENG-11797.
- [15] S.E. Dlugosz, J.W. Fisher, Calibration Study of Heavy Head a325 Bolts, Fritz Engineering Laboratory, Department of Civil Engineering, Lehigh University, 1962.
- [16] A. Elkady, Response characteristics of flush end-plate connections, Eng. Struct. 269 (2022) 114856, https://doi.org/10.1016/j.engstruct.2022.114856.
- [17] A. Elkady, Bolt Connector App. https://github.com/amaelkady/Bolt-Connector-App, 2025.
- [18] A. Elkady, L. Mak, Data driven evaluation of existing numerical modelling guidelines for semi-rigid connections, in: Proc., International Conference on the Behaviour of Steel Structures in Seismic Areas, 2022, pp. 244–251.

- [19] EN-14399-4, High-Strength Structural Bolting Assemblies for Preloading Part 4: System Hv – Hexagon Bolt and Nut Assemblies, European Committee for Standardization, Brussels, Belgium, 2015.
- [20] L. Gödrich, F. Wald, J. Kabeláč, M. Kuříková, Design finite element model of a bolted t-stub connection component, J. Constr. Steel Res. 157 (2019) 198–206, https://doi.org/10.1016/j.jcsr.2019.02.031.
- [21] E.L. Grimsmo, A. Aalberg, M. Langseth, A.H. Clausen, Failure modes of bolt and nut assemblies under tensile loading, J. Constr. Steel Res. 126 (2016) 15–25, https:// doi.org/10.1016/j.jcsr.2016.06.023.
- [22] E.L. Grimsmo, A.H. Clausen, M. Langseth, A. Aalberg, An experimental study of static and dynamic behaviour of bolted end-plate joints of steel, Int. J. Impact Eng. 85 (2015) 132–145, https://doi.org/10.1016/j.ijimpeng.2015.07.001.
- [23] F. Hanus, G. Zilli, J.-M. Franssen, Behaviour of grade 8.8 bolts under natural fire conditions—tests and model, J. Constr. Steel Res. 67 (8) (2011) 1292–1298, https://doi.org/10.1016/j.jcsr.2011.03.012.
- [24] Y. Hu, L. Shen, S. Nie, B. Yang, W. Sha, Fe simulation and experimental tests of high-strength structural bolts under tension, J. Constr. Steel Res. 126 (2016) 174–186, https://doi.org/10.1016/j.jcsr.2016.07.021.
- [25] ISO-898, "Iso 898–1: Mechanical Properties of Fasteners made of Carbon Steel Alloy Steel." Sitzerland, 2013.
- [26] N. Jankovic, F. Ljubinkovic, J. Conde, C. Jordi, L.S. da Silva, Behaviour and design resistance of long bolts in tension, J. Constr. Steel Res. 229 (2025) 109492, https://doi.org/10.1016/j.jcsr.2025.109492.
- [27] G. Kendall, A. Belyi, A. Elkady, Experimental investigation of welded steel t-stub components under high loading rates, J. Constr. Steel Res. 220 (2024) 108851, https://doi.org/10.1016/j.jcsr.2024.108851.
- [28] D. Li, B. Uy, J. Wang, Y. Song, Behaviour and design of grade 10.9 high-strength bolts under combined actions, Steel Compos. Struct. 35 (3) (2020) 327–341, https://doi.org/10.12989/scs.2020.35.3.327.
- [29] D. Li, B. Uy, J. Wang, Y. Song, Behaviour and design of high-strength grade 12.9 bolts under combined tension and shear, J. Constr. Steel Res. 174 (2020) 106305, https://doi.org/10.1016/j.jcsr.2020.106305.
- [30] L. Mak, A. Elkady, Experimental database for steel flush end-plate connections, J. Struct. Eng. 147 (7) (2021) 04721006, https://doi.org/10.1061/(ASCE)ST.1943-541X.0003064.
- [31] A.M. Moore, Evaluation of the Current Resistance Factors for High-Strength Bolts, University of Cincinnati, 2007.
- [32] H. Munter, Proposal for the standardiation of extended end plate connections based on test results. Tests and analysis, 1983.
- [33] P.N.G. Nogueiro, Comportamento Cíclico de Ligações Metálicas, Instituto Politecnico de Braganca (Portugal), 2009.
- [34] X. Qiang, F.S. Bijlaard, H. Kolstein, X. Jiang, Behaviour of beam-to-column high strength steel endplate connections under fire conditions-part 1: experimental

- study, Eng. Struct. 64 (2014) 23–38, https://doi.org/10.1016/j.engstruct.2014.01.028.
- [35] L. Rölle, Das trag-und verformungsverhalten geschraubter stahl-und verbundknoten bei vollplastischer bemessung und in außergewöhnlichen bemessungssituationen, 2013.
- [36] V.V. Saykin, T.H. Nguyen, J.F. Hajjar, D. Deniz, J. Song, The effect of triaxiality on finite element deletion strategies for simulating collapse of full-scale steel structures, Eng. Struct. 210 (2020) 110364, https://doi.org/10.1016/j. engstruct.2020.110364.
- [37] F. Schauwecker, D. Moncayo, P. Middendorf, Characterization of high-strength bolts and the numerical representation method for an efficient crash analysis, Eng. Fail. Anal. 137 (2022) 106249, https://doi.org/10.1016/j. engfailanal\_2022\_106249.
- [38] G. Shi, Y. Shi, Y. Wang, Behaviour of end-plate moment connections under earthquake loading, Eng. Struct. 29 (5) (2007) 703–716, https://doi.org/10.1016/ j.engstruct.2006.06.016.
- [39] Y. Song, Behaviour and Design of Stainless Steel and Stainless Steel-Concrete Composite Beam-to-Column Joints with End-Plate Connections, The University of Sydney, 2022.
- [40] Y. Song, J. Wang, B. Uy, D. Li, Experimental behaviour and fracture prediction of austenitic stainless steel bolts under combined tension and shear, J. Constr. Steel Res. 166 (2020) 105916, https://doi.org/10.1016/j.jcsr.2019.105916.
- [41] N. Stranghöner, C. Abraham, L. Ehrhardt, New design approaches for tension, shear and interaction resistance of carbon steel bolts, J. Constr. Steel Res. 212 (2024) 108260, https://doi.org/10.1016/j.jcsr.2023.108260.
- [42] J.A. Swanson, Characterization of the Strength, Stiffness, and Ductility Behavior of T-Stub Connections, Georgia Institute of Technology, 1999.
- [43] J.A. Swanson, R.T. Leon, Stiffness modeling of bolted t-stub connection components, J. Struct. Eng. 127 (5) (2001) 498–505, https://doi.org/10.1061/ (ASCE)0733-9445(2001)127:5(498).
- [44] VDI, 2230–1: 2015 systematic calculation of highly stressed bolted joints—joints with one cylindrical bolt, 2015.
- [45] Z. Wu, S. Zhang, S.-F. Jiang, Simulation of tensile bolts in finite element modeling of semi-rigid beam-to-column connections, Int. J. Steel Struct. 12 (2012) 339–350, https://doi.org/10.1007/s13296-012-3004-8.
- [46] F. Yang, M. Veljkovic, Y. Liu, Fracture simulation of partially threaded bolts under tensile loading, Eng. Struct. 226 (2021) 111373, https://doi.org/10.1016/j. engstruct.2020.111373.
- [47] S. Yang, Y. Zhu, R. Zhang, Y. Zhao, H. Yang, Rate-dependent behaviour of high-strength steel bolts, J. Constr. Steel Res. 215 (2024) 108560, https://doi.org/ 10.1016/j.icsr.2024.108560.
- [48] X. Zhao, S. He, S. Yan, Full-range behaviour of t-stubs with various yield line patterns, J. Constr. Steel Res. 186 (2021) 106919, https://doi.org/10.1016/j. jcsr.2021.106919.